No. 659 **January 2023**

Robust Monolithic Multigrid FEM Solver for Three Field Formulation of Incompressible Flow Problems

M. A. Afaq, A. Fatima, S. Turek, A. Ouazzi

ISSN: 2190-1767

Robust Monolithic Multigrid FEM Solver for Three Field Formulation of Incompressible Flow Problems

M. A. Afaq*, A. Fatima, S. Turek and A. Ouazzi

Institute for Applied Mathematics, LS III, TU Dortmund University,
Vogelpothsweg 87, 44227, Dortmund, Germany
** aaqib.afaq@math.tu-dortmund.de, arooj.fatima@math.tu-dortmund.de*
stefan.turek@math.tu-dortmund.de, abderrahim.ouazzi@math.tu-dortmund.de.

Abstract

Numerical simulation of three field formulations of incompressible flow problems is of interest for many industrial applications, for instance macroscopic modeling of Bingham, viscoelastic and multiphase flows, which usually consists in supplementing the mass and momentum equations with a differential constitutive equation for the stress field. The variational formulation rising from such continuum mechanics problems leads to a three field formulation with saddle point structure. The solvability of the problem requires different compatibility conditions (LBB conditions) [1] to be satisfied. Moreover, these constraints over the choice of the spaces may conflict/challenge the robustness and the efficiency of the solver. For illustrating the main points, we will consider the three field formulation of the Navier-Stokes problem in terms of velocity, stress, and pressure. Clearly, the weak form imposes the compatibility constraints over the choice of velocity, stress, and pressure spaces. So far, the velocity-pressure combination took much more attention from the numerical analysis and computational fluid dynamic community, which leads to some best interpolation choices for both accuracy and efficiency, as for instance the combination Q_2/P_1^{disc}.

To maintain the computational advantages of the Navier-Stokes solver in two field formulations, it may be more suitable to have a Q_2 interpolation for the stress as well, which is not stable in the absence of pure viscous term [2]. We proceed by adding an edge oriented stabilization to overcome such situation. Furthermore, we show the robustness and the efficiency of the resulting discretization in comparison with the Navier-Stokes solver both in two field as well as in three field formulation in the presence of pure viscous term. Moreover, the benefit of adding the edge oriented finite element stabilization (EOFEM) [3, 4] in the absence of the pure viscous term is tested.

The nonlinearity is treated with a Newton-type solver [5] with divided difference evaluation of the Jacobian matrices [6, 7]. The resulting linearized system inside of the outer Newton solver is a typical saddle point problem which is solved using a geomet-

rical multigrid method with Vanka-like smoother [8, 9]. The method is implemented into the FeatFlow [10] software package for the numerical simulation. The stability and robustness of the method is numerically investigated for "flow around cylinder" benchmark [7, 11].

Keywords: Finite element method, Navier-Stokes equations, Babuska-Brezzi conditions, Edge oriented stabilization

---

1. INTRODUCTION

Numerical simulation of three field formulation is of interest for many industrial applications for instance macroscopic modeling of Bingham, viscoelastic and multiphase flows, which usually consists in supplementing the mass and momentum equations with a differential constitutive equation for the stress field. The variational formulation rising from such continuum mechanics problems leads to a three field formulation with saddle point structure. The three field system of Navier-Stokes equations is given as

$$\begin{cases} \boldsymbol{\sigma} - 2\eta \mathbf{D}(\boldsymbol{u}) = 0 & \text{in } \Omega, \\ \boldsymbol{u} \cdot \nabla \boldsymbol{u} - \nabla \cdot \Big(2\eta(1-\alpha)\mathbf{D}(\boldsymbol{u}) + \alpha \boldsymbol{\sigma} \Big) + \nabla p = 0 & \text{in } \Omega, \\ \nabla \cdot \boldsymbol{u} = 0 & \text{in } \Omega, \\ \boldsymbol{u} = \boldsymbol{g}_D & \text{on } \Gamma_D. \end{cases} \tag{1}$$

Here, $\boldsymbol{\sigma}$ is the extra stress tensor, $\mathbf{D} = \frac{1}{2}(\nabla u + (\nabla u)^{\mathrm{T}})$ is the strain rate tensor, $\boldsymbol{u}$ is the velocity, η is the viscosity, p is the pressure. Moreover, α is a parameter which denotes the contribution of the solvent viscosity. The range of this parameter is $0 \leq \alpha \leq 1$, where $\alpha = 1$ corresponds to the zero solvent viscosity (which often occurs in the case of viscoelastic fluids).

2. VARIATIONAL FORMULATIONS

For solving the system of equations (1) with finite element method, we will first multiply the equations with the test functions ($\boldsymbol{\tau}$, $\boldsymbol{v}$, q) and using integration by parts, we obtain the weak formulation as follows:

$$\begin{aligned} \int_\Omega \Big(\boldsymbol{\sigma} : \boldsymbol{\tau} \Big) dx - \int_\Omega 2\eta \Big(\mathbf{D}(\boldsymbol{u}) : \boldsymbol{\tau} \Big) dx = 0 \quad & \text{in } \Omega, \\ \int_\Omega (\boldsymbol{u} \cdot \nabla \boldsymbol{u}) \boldsymbol{v} \, dx + \int_\Omega \Big(2\eta(1-\alpha)\mathbf{D}(\boldsymbol{u}) : \mathbf{D}(\boldsymbol{v}) \Big) dx + \int_\Omega \Big(\alpha \boldsymbol{\sigma} : \mathbf{D}(\boldsymbol{v}) \Big) dx - \int_\Omega p \nabla \cdot \boldsymbol{v} dx = 0 \quad & \text{in } \Omega, \\ \int_\Omega \Big(\nabla \cdot \boldsymbol{u} \Big) q dx = 0 \quad & \text{in } \Omega. \end{aligned} \tag{2}$$

Let $\mathbb{V} = \boldsymbol{H}_0^1(\Omega) := \left(H_0^1(\Omega)\right)^2$, $\mathbb{Q} = L_0^2(\Omega)$, and $\mathbb{T} = \left(L^2(\Omega)\right)^{2\times 2}_{\text{sym}}$ be the spaces for the velocity, pressure, and stress, respectively, and let $\mathbb{V}'$, $\mathbb{Q}'$, and $\mathbb{T}'$ be their corresponding dual spaces. Furthermore, we set $\mathbb{Y} := \mathbb{V} \times \mathbb{T}$ and $\mathbb{Y}' := \mathbb{V}' \times \mathbb{T}'$. We introduce the following linear forms: $\mathcal{A}_{\boldsymbol{\sigma}}$ is defined on $\mathbb{T} \to \mathbb{T}'$ as follows:

$$\langle \mathcal{A}_{\boldsymbol{\sigma}} \boldsymbol{\sigma}, \boldsymbol{\tau} \rangle = \alpha \int_\Omega \boldsymbol{\sigma} : \boldsymbol{\tau} \, dx, \quad \forall \boldsymbol{\sigma}, \boldsymbol{\tau} \in \mathbb{T}, \tag{3}$$

and the associated bilinear form defined on $\mathbb{T} \times \mathbb{T} \longrightarrow \mathbb{R}$

$$a_{\boldsymbol{\sigma}}(\boldsymbol{\sigma}, \boldsymbol{\tau}) = \langle \mathcal{A}_{\boldsymbol{\sigma}} \boldsymbol{\sigma}, \boldsymbol{\tau} \rangle, \tag{4}$$

$\mathcal{N}_{\boldsymbol{u}}$ and $\mathcal{L}_{\boldsymbol{u}}$ are defined on $\mathbb{V} \longrightarrow \mathbb{V}'$ as follows:

$$\langle \mathcal{N}_{\boldsymbol{u}} \boldsymbol{u}, \boldsymbol{v} \rangle = \int_\Omega (\boldsymbol{u} \cdot \nabla \boldsymbol{u}) \boldsymbol{v} \, dx, \quad \forall \boldsymbol{u}, \boldsymbol{v}, \in \mathbb{V}, \tag{5}$$

$$\langle \mathcal{L}_{\boldsymbol{u}} \boldsymbol{u}, \boldsymbol{v} \rangle := 2\eta(1-\alpha) \int_\Omega \mathbf{D}(\boldsymbol{u}) : \mathbf{D}(\boldsymbol{v}) \, dx, \quad \forall \boldsymbol{u}, \boldsymbol{v} \in \mathbb{V}, \tag{6}$$

we set

$$\mathcal{A}_{\boldsymbol{u}} := \mathcal{L}_{\boldsymbol{u}} + \mathcal{N}_{\boldsymbol{u}}, \tag{7}$$

and the associated bilinear form defined on $\mathbb{V} \times \mathbb{V} \longrightarrow \mathbb{R}$

$$a_{\boldsymbol{u}}(\boldsymbol{u}, \boldsymbol{v}) = \langle \mathcal{A}_{\boldsymbol{u}} \boldsymbol{u}, \boldsymbol{v} \rangle. \tag{8}$$

$\mathcal{B}$ and $\mathcal{C}$ defined on $\mathbb{V} \longrightarrow \mathbb{Q}'$ respectively, $\mathbb{V} \longrightarrow \mathbb{T}'$

$$\langle \mathcal{B}\boldsymbol{v}, q \rangle := -\int_\Omega \nabla \cdot \boldsymbol{v} \; q \, dx, \tag{9}$$

respectively,

$$\langle \mathcal{C}\boldsymbol{v}, \boldsymbol{\tau} \rangle := 2\eta\alpha \int_\Omega \boldsymbol{\tau} : \mathbf{D}(\boldsymbol{v}) \, dx, \tag{10}$$

with the associated bilinear forms $b(\cdot,\cdot)$ and $c(\cdot,\cdot)$ defined on $\mathbb{V} \times \mathbb{Q} \longrightarrow \mathbb{R}$ and $\mathbb{V} \times \mathbb{T} \longrightarrow \mathbb{R}$ respectively, read:

$$b(\boldsymbol{v}, q) := \left\langle \mathcal{B}\boldsymbol{v}, q \right\rangle, \tag{11}$$

respectively,

$$c(\boldsymbol{v}, \boldsymbol{\tau}) := \left\langle \mathcal{C}\boldsymbol{v}, \boldsymbol{\tau} \right\rangle. \tag{12}$$

We define the bilinear forms $a(\cdot,\cdot)$ defined on $\mathbb{Y} \times \mathbb{Y} \longrightarrow \mathbb{R}$ and $b(\cdot,\cdot)$ defined on $\mathbb{Y} \times \mathbb{Q} \longrightarrow \mathbb{R}$ reads; for $\mathcal{U} = (\boldsymbol{u}, \boldsymbol{\sigma})$ and $\mathcal{V} = (\boldsymbol{v}, \boldsymbol{\tau})$

$$\begin{aligned} a(\mathcal{U}, \mathcal{V}) =& \langle \mathcal{A}_{\boldsymbol{u}} \boldsymbol{u}, \boldsymbol{v} \rangle + \langle \mathcal{A}_{\boldsymbol{\sigma}} \boldsymbol{\sigma}, \boldsymbol{\tau} \rangle + \left\langle \mathcal{C}\boldsymbol{v}, \boldsymbol{\sigma} \right\rangle + \left\langle \mathcal{C}^T \boldsymbol{u}, \boldsymbol{\tau} \right\rangle, \\ b(\mathcal{U}, q) =& b(\boldsymbol{u}, q). \end{aligned} \tag{13}$$

The compact weak formulation for the three field Navier-Stokes system (1) reads:
Find $(\mathcal{U}, p) \in \mathbb{Y} \times \mathbb{Q}$ *s.t.*

$$\begin{cases} a(\mathcal{U}, \mathcal{V}) + b(\mathcal{V}, p) = 0 & \forall \mathcal{V} \in \mathbb{Y}, \\ b(\mathcal{U}, q) = 0 & \forall q \in \mathbb{Q}. \end{cases} \tag{14}$$

3. FINITE ELEMENT APPROXIMATION

For the space discretization, let the bounded domain $\Omega \subset \mathbb{R}^d$ be partitioned by a *grid* $\mathcal{T}_h$ consisting of elements $K \in \mathcal{T}_h$ which are assumed to be open quadrilaterals such that $\Omega = \mathrm{int}\big(\bigcup_{K\in\mathcal{T}_h} \overline{K}\big)$. For an element $K \in \mathcal{T}_h$, we denote by $\mathcal{E}(K)$ the set of all 1-dimensional edges of K. Let $\mathcal{E}_i := \bigcup_{k\in\mathcal{T}_h} \mathcal{E}(K)$ be the set of all interior element edges of the grid $\mathcal{T}_h$. The approximation of the problems (14) with the finite element method, we introduce the approximation spaces $\mathbb{V}^h$, $\mathbb{T}^h$ and $\mathbb{Q}^h$ of $\mathbb{V}$, $\mathbb{T}$ and $\mathbb{Q}$ and define the product space $\mathbb{Y}^h := \mathbb{V}^h \times \mathbb{T}^h$.

$$\begin{aligned} \mathbb{V}^h &= \left\{ \boldsymbol{v}_h \in \mathbb{V}, \boldsymbol{v}_{h|K} \in (Q_2(K))^2 \right\}, \\ \mathbb{T}^h &= \left\{ \boldsymbol{\tau}_h \in \mathbb{T}, \boldsymbol{\tau}_{h|K} \in Q_2(K) \right\}, \\ \mathbb{Q}^h &= \left\{ q_h \in \mathbb{Q}, q_{h|K} \in P_1^{\mathrm{disc}}(K) \right\}. \end{aligned} \tag{15}$$

The velocity and pressure fields are discretized using higher order stable Q_2/P_1^{disc} [12, 13] FEM and Q_2 for the stress variable, presented in Fig. 1.

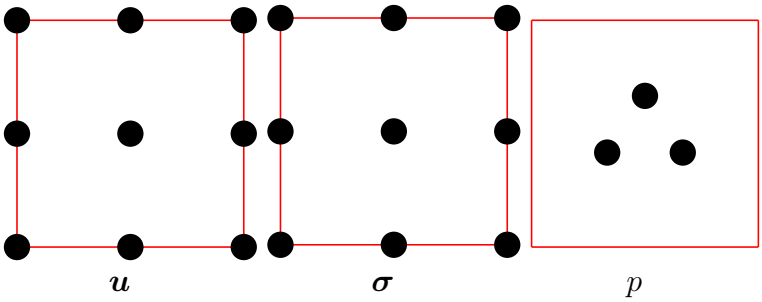

Figure 1: Higher order finite element $Q_2, Q_2, P_1^{\mathrm{disc}}$ on quadrilaterals.

The approximate problem of (14) reads; *Find* $(\mathcal{U}_h, p_h) \in \mathbb{Y}^h \times \mathbb{Q}^h$ *s.t.*

$$\begin{cases} a(\mathcal{U}_h, \mathcal{V}_h) + b(\mathcal{V}_h, p_h) = 0 & \forall \mathcal{V}_h \in \mathbb{Y}^h, \\ b(\mathcal{U}_h, q_h) = 0 & \forall q_h \in \mathbb{Q}^h. \end{cases} \tag{16}$$

The choices of the finite element spaces $\mathbb{V}^h$ and $\mathbb{Q}^h$ satisfy the inf-sup condition. The corresponding nonlinear system reads

$$\begin{bmatrix} \mathcal{A}_{\boldsymbol{u}} & \mathcal{C} & \mathcal{B}^{\mathrm{T}} \\ \mathcal{C}^{\mathrm{T}} & -\mathcal{A}_{\boldsymbol{\sigma}} & \mathbf{0} \\ \mathcal{B} & \mathbf{0} & \mathbf{0} \end{bmatrix} \begin{bmatrix} \boldsymbol{u} \\ \boldsymbol{\sigma} \\ p \end{bmatrix} = \begin{bmatrix} rhs_{\boldsymbol{u}} \\ rhs_{\boldsymbol{\sigma}} \\ rhs_p \end{bmatrix}. \tag{17}$$

4. THE CHOICE OF FINITE ELEMENT SPACE

The choice for FEM spaces for the (Navier)Stokes problem depends on the well known compatibility condition between velocity and pressure spaces, know as inf-sup condition [14]

$$\sup_{\boldsymbol{u}\in\boldsymbol{v}_h} \frac{\int_\Omega div\boldsymbol{u} q dx}{\| \boldsymbol{u} \|_{1,\Omega}} \geq \beta \| q \|_{0,\Omega} \quad \forall q \quad \in \mathbb{Q}^h. \tag{18}$$

The selected finite element pair $Q_2P_1^{disc}$ is compatible according to the equation (18). The study of Baranger et. al. [2] has shown that the choice of the element for stress variable ($\boldsymbol{\sigma}$) can be made depending on the value of α in system of equations (1). It is stated, that the use of the discrete three field Stokes's problem with $0 < \alpha < 1$ (excluding the case $\alpha = 1$) allows to suppress the inf-sup condition on $(\boldsymbol{u}, \boldsymbol{\sigma})$, which broadens the spectrum for choosing the element approximation for extra stress tensor $\boldsymbol{\sigma}$.

Remark: The basic idea is that there is no need of an inf-sup condition on $(\boldsymbol{u}, \boldsymbol{\sigma})$, provided $0 < \alpha < 1$.

The case of $\alpha = 1$ is discussed in the work of Fortin and Pierre [15], which proves that the discrete three field Stokes's problem (16) is well posed and the solution approximates the continuous problem (14), if the following two conditions are satisfied:

- Inf-sup condition on $(\boldsymbol{u}, p)$

$$\inf_{q \in \mathbb{Q}^h} \sup_{\boldsymbol{u} \in \mathbb{V}^h} \frac{(\nabla \cdot \boldsymbol{u}_h, q_h)}{\| \boldsymbol{u}_h \|_1 \| q_h \|_0} \geq \beta > 0. \tag{19}$$

- Inf-sup condition on $(\boldsymbol{u}, \boldsymbol{\sigma})$: Either $\mathbf{D}(\mathbb{V}_h) \subset \mathbb{T}_h$ (in the case of discontinuous $\boldsymbol{\tau}_h$) or the number of interior degrees of freedom for $\boldsymbol{\tau}_h$ in each K is greater or equal to the number of all degrees of freedom of $\boldsymbol{v}_h$ in each K (in the case of continuous $\boldsymbol{\tau}_h$).

$\| \cdot \|_1$ and $\| \cdot \|_0$ are the standard $\boldsymbol{H}_0^1(\Omega)$ and $L_0^2(\Omega)$ norms. In the present study, the stress $\boldsymbol{\sigma}$ is discretized using continuous finite element Q_2, which does not satisfy the second inf-sup condition. Therefore, the edge oriented finite element (EOFEM) stabilization [4] term $J_{\boldsymbol{u}}(\boldsymbol{u}_h, \boldsymbol{v}_h)$ is added in the absence of the solvent viscosity (i.e. $\alpha = 1$). This stabilization penalizes the jump of the solution gradient over the edge $\mathcal{E}$ of the neighbouring elements. The beneficial effects of adding this stabilization are shown in the numerical studies carried out in the next section.

$$J_{\boldsymbol{u}}(\boldsymbol{u}_h, \boldsymbol{v}_h) = \gamma_{\boldsymbol{u}} \sum_{e \in \mathcal{E}_h} 2\eta\alpha h \int_e [\nabla \boldsymbol{u}_h] : [\nabla \boldsymbol{v}_h] \, d\Omega. \tag{20}$$

The corresponding discrete system after the addition of the jump term reads:

$$\begin{bmatrix} \mathcal{A}_{\boldsymbol{u}} + J_{\boldsymbol{u}} & \mathcal{C} & \mathcal{B}^{\mathrm{T}} \\ \mathcal{C}^{\mathrm{T}} & -\mathcal{A}_{\boldsymbol{\sigma}} & \mathbf{0} \\ \mathcal{B} & \mathbf{0} & \mathbf{0} \end{bmatrix} \begin{bmatrix} \boldsymbol{u} \\ \boldsymbol{\sigma} \\ p \end{bmatrix} = \begin{bmatrix} rhs_{\boldsymbol{u}} \\ rhs_{\boldsymbol{\sigma}} \\ rhs_p \end{bmatrix}. \tag{21}$$

5. FLOW AROUND CYLINDER BENCHMARK

This 2-dimensional DFG benchmark [11] analyses the attributes of the flow around an obstacle in a rectangular channel, where a cylinder of radius $r = 0.05$ is placed with the center at $(0.2, 0.2)$ in a rectangular channel of length 2.2, the upper and lower walls are 0.41 length apart. The geometrical configuration and coarse mesh are shown in Fig. 2 and 3. The fluid density (ρ) and kinematic viscosity (η) are set to 1 and 0.001, respectively.

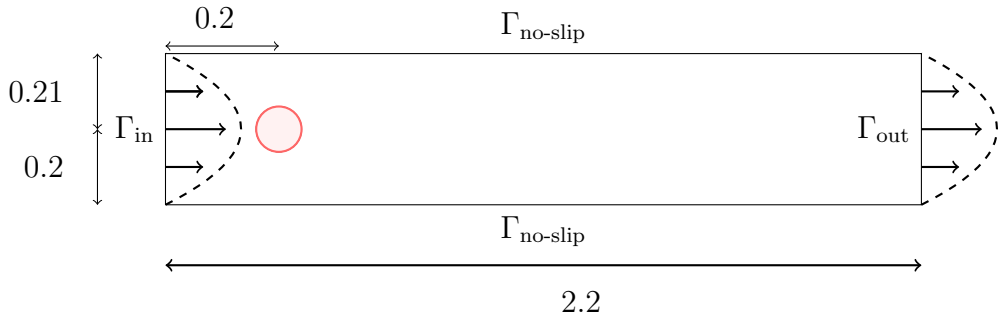

Figure 2: Flow around cylinder configuration.

Dirichlet boundary is defined at the inlet Γ_{in} with a parabolic profile

$$u_x(y) = \Big(\frac{4.0U_{\max}y(0.41-y)}{(0.41)^2}, 0\Big),$$

having maximum velocity $U_{\max} = 0.3$. The corresponding mean velocity $\mathcal{U}_{\text{mean}}$ is defined as

$$\mathcal{U}_{\text{mean}} = \frac{2}{3}U_{\max}.$$

No slip boundary condition is defined at the upper and lower walls and do-nothing boundary condition is defined at the outlet Γ_{out}. The characteristic length of the cylinder ($L = 2r_c = 0.1$) along with the viscosity (η) and mean velocity yields the Reynolds number $Re = 20$, depicting a laminar flow. Here r_c is the radius of the cylinder.

$$\text{R}e = \frac{\mathcal{U}_{\text{mean}}L}{\eta}. \tag{22}$$

Force acting on cylinder surface has two components i.e. lift and drag, respectively. Lift is perpendicular to the direction of flow, whereas drag is parallel to the direction of flow. The mathematical expressions for lift and drag are defined as:

$$\mathcal{F}_L = -\int_{\mathcal{S}}(\eta\frac{\partial \boldsymbol{u_\tau}}{\partial n}n_1 - pn_2)ds, \qquad \mathcal{F}_D = \int_{\mathcal{S}}(\eta\frac{\partial \boldsymbol{u_\tau}}{\partial n}n_2 - pn_1)ds. \tag{23}$$

The dimensionless drag and lift coefficients are also calculated with following definitions

$$C_D = \frac{2}{U_{\text{mean}}^2 L} F_D, \qquad C_L = \frac{2}{U_{\text{mean}}^2 L} F_L.$$

5.1. ***Numerical results***

For testing the robustness and the efficiency of the resulting discretization in comparison with the Navier-Stokes solver both in two field as well as in three field formulation, we substitute $\alpha = 0$, for reducing this system of equations into two field formulation. The numerical results illustrating the performance of system (1) for flow around cylinder benchmark are presented in Table [1]. Numerical results in the form of lift/drag are compared and validated with the reference values [11],

$$C_D = 5.57953523384, \qquad C_L = 0.010618948146,$$

and with the results of Damanik [7]. Convergence of the solution is presented for higher order finite elements (Q_2/P_1^{disc}). Here, "NL" denotes nonlinear iterations, "LL" denotes the average number of multigrid iterations. Each refinement level shows a strong agreement with the reference results. The accuracy of the solution in terms of velocity magnitude, pressure and stream functions are presented in Fig. 4.

However, the basic purpose of this numerical study is to show the suppression of the inf-sup condition on velocity-stress $(\boldsymbol{u}, \boldsymbol{\sigma})$ for the range of α between 0 and 1. Therefore, a detailed study is carried out in Table [2] to show the stability of the three field system, unless $\alpha \to 1$. One can see the accuracy of the solution as well as the robustness of the monolithic Newton-multigrid solver in the above mentioned table. Moreover, these results obtained from higher order finite elements show mesh convergence with respect to the mesh refinements. For the extreme cases, when the solvent viscosity is nearly zero or absent i.e. $0.88 < \alpha \leq 1$, the solver is not able to converge at all because the finite element pair for velocity-stress $(\boldsymbol{u}, \boldsymbol{\sigma})$ is not stable. In order to circumvent this stability issue, edge oriented stabilization is added by setting "$\gamma = 10^{-4}$", which clearly shows that the solver is able to achieve nearly accurate results as well as the behaviour of convergence is quite good with the decent number of iterations.

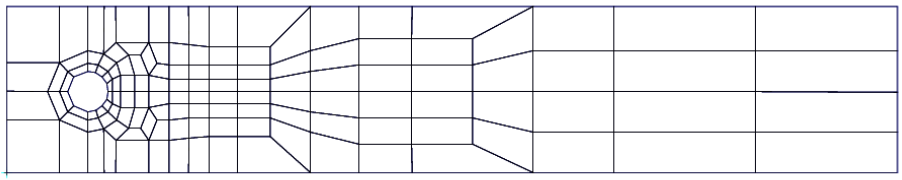

Figure 3: Flow around cylinder coarse mesh.

Table 1: **Navier-Stokes**: Validation of the lift and drag values of the flow around cylinder in a rectangular channel. "NL" denotes nonlinear iterations, "LL" denotes the average number of multigrid iterations. L.I. and V.I. stands for the line and volume integral.

	L.I.		**V.I.**			**Damanik (L.I.) [7]**		
Level	Lift	Drag	Lift	Drag	NL/LL	Lift	Drag	NL/LL
1	0.009497543	5.5550	0.009447476	5.5424	9/1	0.009498	5.5550	9/2
2	0.010600652	5.5722	0.010468846	5.5672	9/1	0.010601	5.5722	9/2
3	0.010615639	5.5776	0.010567879	5.5761	9/1	0.010616	5.5776	9/1
4	0.010617798	5.5791	0.010603975	5.5787	8/1	0.010618	5.5790	8/1
5	0.010618726	5.5794	0.010615029	5.5793	7/1			

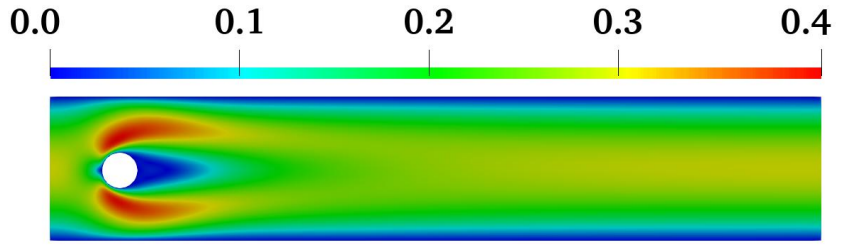

(a) Velocity magnitude

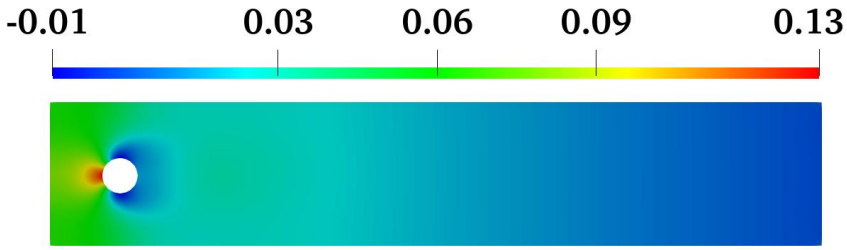

(b) Pressure distribution

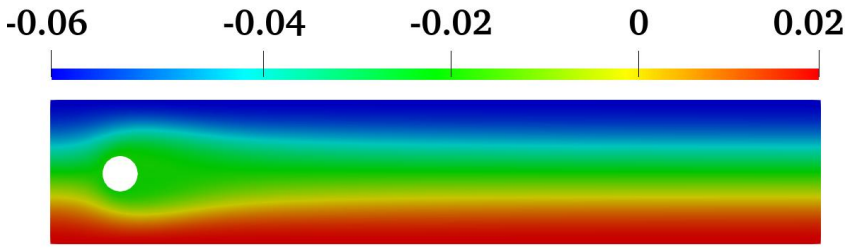

(c) Stream function

Figure 4: Flow around cylinder: Visualization of the velocity, pressure and stream function.

Table 2: **Navier-Stokes**: Effect of the EOFEM stabilization on the lift and drag values of the flow around cylinder in a rectangular channel. "NL" denotes nonlinear iterations, "LL" denotes the average number of multigrid iterations. The results are calculated at different mesh refinement levels for different values of α, the tolerance criteria of the linear solver is set to 10^{-3}.

					With EOFEM		
α	Level	Lift	Drag	NL/LL	Lift	Drag	NL/LL
0	1	0.008786117	5.5285	7/4	0.010107982	5.5427	7/3
0	2	0.010424275	5.5663	7/4	0.010702943	5.5674	7/3
0	3	0.010597517	5.5764	7/3	0.010619474	5.5757	7/3
0	4	0.010615911	5.5788	7/4	0.010616941	5.5782	7/3
0	5	0.010618494	5.5794	7/4	0.010618268	5.5790	6/4
0.25	1	0.009307183	5.5454	7/3	0.010013472	5.5301	7/3
0.25	2	0.010559395	5.5701	7/2	0.010677420	5.5639	7/2
0.25	3	0.010611104	5.5772	7/2	0.010615166	5.5744	7/3
0.25	4	0.010617270	5.5790	7/2	0.010615982	5.5777	7/3
0.25	5	0.010618658	5.5794	6/3	0.010617947	5.5788	6/4
0.5	1	0.009075847	5.5363	7/3	0.009911587	5.5171	7/3
0.5	2	0.010506223	5.5681	7/3	0.010650185	5.5601	7/2
0.5	3	0.010605621	5.5767	7/3	0.010610603	5.5730	7/3
0.5	4	0.010616682	5.5789	7/3	0.010614926	5.5771	7/3
0.5	5	0.010618582	5.5794	7/3	0.010617576	5.5785	7/4
0.75	1	0.008786117	5.5285	7/4	0.009800026	5.5039	7/3
0.75	2	0.010424275	5.5663	7/4	0.010620649	5.5562	7/3
0.75	3	0.010597517	5.5764	7/3	0.010605686	5.5715	7/3
0.75	4	0.010615911	5.5788	7/4	0.010613740	5.5764	7/3
0.75	5	0.010618494	5.5794	7/4	0.010617138	5.5782	7/4
0.88	1	0.008605515	5.5268	8/6	0.009737168	5.4969	7/3
0.88	2	0.010352916	5.5652	7/6	0.010604083	5.5541	7/3
0.88	3	0.010589597	5.5762	7/6	0.010602939	5.5706	7/3
0.88	4	0.010615198	5.5788	7/7	0.010613035	5.5760	6/3
0.88	5	0.010618421	5.5794	7/8	0.010616876	5.5780	7/4
1	1	-	-	-	0.009675569	5.4903	7/3
1	2	-	-	-	0.010587841	5.5520	7/3
1	3	-	-	-	0.010600252	5.5698	7/3
1	4	-	-	-	0.010612372	5.5756	7/3
1	5	-	-	-	0.010616606	5.5778	7/4

To obtain even more accurate drag and lift coefficients, a comparison study for the optimal value of the stabilization parameter "γ" is carried out for vanishing viscosity cases ($\alpha = 0.9, 1.0$) presented in Table [3] and Table [4]. For the extreme case ($\alpha = 1.0$), the solver does not converge for $\gamma < 10^{-5}$. From these tables, it is concluded that "$\gamma = 10^{-4}$" is the optimal value of the stabilization parameter, which gives not only the accurate desired quantities but also faster convergence rate of the solver. Hence, the three field Navier-Stokes solver is robust and accurate.

Table 3: **Navier-Stokes**: Lift and drag values of the flow around cylinder in a rectangular channel, $\alpha = 0.9$. "NL" denotes nonlinear iterations, "LL" denotes the average number of multigrid iterations. L.I. and V.I. stands for the line and volume integral.

	L.I.		**V.I.**		
Level	Lift	Drag	Lift	Drag	NL/LL
$\gamma = 10^{-4}$					
1	0.009727154	5.4958	0.009717593	5.5329	7/3
2	0.010601445	5.5537	0.010511472	5.5649	7/3
3	0.010602502	5.5705	0.010566725	5.5756	7/3
4	0.010612946	5.5759	0.010603146	5.5785	7/3
5	0.010616833	5.5779	0.010614868	5.5793	7/5
6	0.010618046	5.5788	0.010617929	5.5795	7/6
$\gamma = 10^{-5}$					
1	0.008943680	5.5110	0.008919255	5.5435	7/4
2	0.010455364	5.5579	0.010375034	5.5665	7/4
3	0.010594742	5.5722	0.010559730	5.5759	7/4
4	0.010613554	5.5766	0.010603219	5.5786	7/4
5	0.010617227	5.5782	0.010614852	5.5793	6/5
6	0.010618268	5.5789	0.010617924	5.5795	7/7
$\gamma = 10^{-6}$					
1	0.008671221	5.5206	0.008599485	5.5477	7/5
2	0.010377576	5.5617	0.010297781	5.5674	7/5
3	0.010590503	5.5742	0.010555386	5.5760	7/5
4	0.010614374	5.5776	0.010603249	5.5786	6/5
5	0.010617850	5.5788	0.010614936	5.5793	6/7
6	0.010618481	5.5792	0.010617860	5.5795	7/9

Table 4: **Navier-Stokes**: Lift and drag values of the flow around cylinder in a rectangular channel, $\alpha = 1.0$. "NL" denotes nonlinear iterations, "LL" denotes the average number of multigrid iterations. L.I. and V.I. stands for the line and volume integral.

	L.I.		**V.I.**		
Level	Lift	Drag	Lift	Drag	NL/LL
$\gamma = 10^{-4}$					
1	0.009675569	5.4903	0.009669980	5.5331	7/3
2	0.010587841	5.5520	0.010503484	5.5650	7/3
3	0.010600252	5.5698	0.010566096	5.5757	7/3
4	0.010612372	5.5756	0.010603133	5.5786	7/3
5	0.010616606	5.5778	0.010614890	5.5793	7/4
6	0.010617940	5.5787	0.010617944	5.5795	7/6
$\gamma = 10^{-5}$					
1	0.008817877	5.5068	0.008778103	5.5454	7/6
2	0.010415676	5.5555	0.010342654	5.5666	7/6
3	0.010589744	5.5712	0.010557220	5.5759	7/6
4	0.010612578	5.5761	0.010603086	5.5786	7/7
5	0.010616837	5.5780	0.010614860	5.5793	7/9
6	0.010618305	5.5788	0.010618128	5.5795	12/10

6. CONCLUSION

In this work, we have presented the study of the three field formulation by adding the constitutive equation of the stress variable $\boldsymbol{\sigma}$ into the classical Navier-Stokes equations. The main focus is to get rid of the inf-sup stability condition for the velocity-stress variable according to the Baranger et al. [2], when the solvent viscosity is present in the system of equations (1), which corresponds to the $0 < \alpha < 1$. This relaxation expands the choice of the discretization element of the stress varaible. Therefore, to maintain the computational advantages of the Navier-Stokes solver in two field formulation, it may be more suitable to have a Q_2 interpolation for the stress as well, which is not stable in the absence of pure viscous term [2]. We proceed by adding an edge oriented stabilization to overcome such situation. Moreover, the benefit of adding this stabilization in the absence of the pure viscous term is tested for the laminar flow around cylinder configuration. The stability and robustness of the method is investigated numerically, where it clearly shows that there is no condition needed for the velocity-stress in the presence of pure viscous term. To fulfill the inf-sup condition in the case of $\alpha = 1$, either we can choose the right finite element or we can add this stabilization with the optimal parameter γ, which does not effect the solution accuracy but on the other hand, also helps the solver to converge smoothly.

The numerical results presented in this article are for Newtonian fluids, however, in future the studies will be carried out for non-Newtonian fluids, which is the basic motivation of the

three field formulation.

ACKNOWLEDGEMENTS

Muhammad Aaqib Afaq would like to thank Erasmus Mundus INTACT project, funded by the European Union as part of the Erasmus Mundus programme and the National University of Sciences and Technology (NUST) for their financial support. The authors also acknowledge the support by LS3 and LiDO3 team at ITMC, TU Dortmund University.

References

[1] V. Girault and P. A. Raviart. *Finite Element Methods for Navier-Stokes equations.* Springer, Berlin-Heidelberg, 1986.

[2] J. Baranger and D. Sandri. A formulation of Stokes's problem and the linear elasticity equations suggested by the Oldroyd model for viscoelastic flow. *M2AN. Mathematical modelling and numerical analysis*, 26(2):331–345, 1992.

[3] A. Ouazzi. *Finite Element Simulation of Nonlinear Fluids: Application to Granular Material and Powder.* Industrial and applied mathematics. Shaker, 2005.

[4] S. Turek and A. Ouazzi. Unified edge–oriented stabilization of nonconforming FEM for incompressible flow problems: Numerical investigations. *Journal of Numerical Mathematics*, 15(4):299–322, 2007.

[5] C. T. Kelley. *Iterative methods for linear and nonlinear equations.* SIAM, Philadelphia, 1995.

[6] H. Damanik, J. Hron, A. Ouazzi, and S. Turek. Monolithic Newton-multigrid solution techniques for incompressible nonlinear flow models. *International Journal for Numerical Methods in Fluids*, 71:208–222, 2012.

[7] H. Damanik. *FEM Simulation of Non-isothermal Viscoelastic Fluids.* TU Dortmund, Germany, 2011. PhD Thesis.

[8] H. Wobker and S. Turek. Numerical studies of vanka-type smoothers in computational solid mechanics. *Advances in Applied Mathematics and Mechanics*, 1(1):29–55, 2009.

[9] S. Turek, M. Griebel, D. Keyes, and R. Nieminen. *Efficient Solvers for Incompressible Flow Problems: An Algorithmic and Computational Approache.* Lecture notes in computational science and engineering. Springer-Verlag, 1999.

[10] Featflow. http://www.mathematik.tu-dortmund.de/ featflow/en/index.html.

[11] DFG benchmark 2D-1 (RE20, laminar). http://www.mathematik.tu-dortmund.de/ featflow/en/benchmarks/cfdbenchmarking/flow/dfgbenchmark1re20.html.

[12] J. Hron, A. Ouazzi, and S. Turek. A computational comparison of two fem solvers for nonlinear incompressible flow. In Eberhard Bänsch, editor, *Challenges in Scientific Computing - CISC 2002*, pages 87–109, "Berlin, Heidelberg", 2003. Springer Berlin Heidelberg.

[13] D. Arnold, D. Boffi, and R. Falk. Approximation by quadrilateral finite elements. *Mathematics of computation*, 71(239):909–922, 2002.

[14] D. S. Malkus. Eigenproblems associated with the discrete LBB condition for incompressible finite elements. *International Journal of Engineering Science*, 19(10):1299–1310, 1981.

[15] M. Fortin and R. Pierre. On the convergence of the mixed method of Crochet and Marchal for viscoelastic flows. *Computer Methods in Applied Mechanics and Engineering*, 73(3):341–350, 1989.